

Journal of Materials Chemistry B

Accepted Manuscript



This is an *Accepted Manuscript*, which has been through the Royal Society of Chemistry peer review process and has been accepted for publication.

Accepted Manuscripts are published online shortly after acceptance, before technical editing, formatting and proof reading. Using this free service, authors can make their results available to the community, in citable form, before we publish the edited article. We will replace this *Accepted Manuscript* with the edited and formatted *Advance Article* as soon as it is available.

You can find more information about *Accepted Manuscripts* in the [Information for Authors](#).

Please note that technical editing may introduce minor changes to the text and/or graphics, which may alter content. The journal's standard [Terms & Conditions](#) and the [Ethical guidelines](#) still apply. In no event shall the Royal Society of Chemistry be held responsible for any errors or omissions in this *Accepted Manuscript* or any consequences arising from the use of any information it contains.



ARTICLE

Photosensitizer-Loaded Bubble-Generating Mineralized Nanoparticles for Ultrasound Imaging and Photodynamic Therapy

Received 00th January 20xx,
Accepted 00th January 20xx

DOI: 10.1039/x0xx00000x

www.rsc.org/

Dong Jin Park,^{†a} Kyung Hyun Min,^{†a} Hong Jae Lee,^b Kwangmeyung Kim,^c Ick Chan Kwon,^c Seo Young Jeong^a and Sang Cheon Lee^{*b}

In this work, we have developed photosensitizer-loaded bubble-generating calcium carbonate (CaCO₃)-mineralized nanoparticles that have a potential for ultrasound imaging (US)-guided photodynamic therapy (PDT) of tumors. A photosensitizer, chlorin e6 (Ce6)-loaded CaCO₃-mineralized nanoparticles (Ce6-BMNs) were prepared by an anionic block copolymer-templated *in situ* mineralization method. The Ce6-BMNs were composed of the Ce6-loaded CaCO₃ core and the hydrated poly(ethylene glycol) (PEG) shell. The Ce6-BMNs exhibited excellent stability under a serum condition. The Ce6-BMNs show enhanced echogenic US signals at tumoral acid pH by generating carbon dioxide (CO₂) bubbles. The Ce6-BMNs effectively inhibited Ce6 release at physiological pH (7.4). At a tumoral acidic pH (6.4), Ce6 release was accelerated with CO₂ bubble generation due to dissolution of the CaCO₃ mineral core. Upon irradiation of Ce6-BMNs-treated MCF-7 breast cancer cells, the cell viability dramatically decreased with increasing Ce6 concentration. The phototoxicity of the Ce6-BMNs was much higher than that of free Ce6. On the basis of tumoral pH-responsive CO₂ bubble-generation and simultaneously Ce6 release at the target tumor site, this CaCO₃ mineralized nanoparticles can be considered as a promising theranostic nanoparticle for US imaging-guided PDT in the field of tumor therapy.

Introduction

Theranostic nanoparticles combining diagnostic imaging and therapeutic functionalities have been extensively developed in the field of nanomedicine for tumor treatment. They have played a significant role in detecting exact location, margin and size of tumors before therapy, and expressed additional therapeutic activities for successful tumor treatment.^[1] Currently, diverse theranostic nanoparticles have been employed for a variety of diagnostic imaging modalities such as magnetic resonance imaging (MRI), positron emission tomography (PET), computed tomography (CT), optical imaging, and ultrasound (US) imaging have been used.^[2] In particular, US imaging, as a non-invasive real-time imaging tool, has unique advantages such as high safety, low cost, and ease access to patients.^[3] With the use of US contrast agents, the improved sensitivity and high resolution of US imaging have been obtained.^[4] Conventional US contrast agents have been developed in a form of microbubbles composed of the inner gas such as perfluorocarbon and the outer shell materials including

proteins, lipids, and polymers.^[4a,5] It is known that perfluorocarbon-encapsulated microbubbles have shown to be easily destroyed by diffusing away of perfluorocarbon at body temperature, which caused the short half-life of contrast agents.^[6] Owing to micro size, low stability, and lack of prolonged circulating properties, their applications are limited for imaging of target tumor tissues.^[4c,7] For this reason, developing effective US contrast agents with long half-life and enhanced stability for the diagnostic use of tumor tissues is a significant challenge in clinical and research fields.

Recently, with a specialty in biomimetically mineralized nanoparticles, we have reported various useful pH-responsive nanoparticle systems to improve anticancer diagnostic and therapeutic activity.^[8] We have developed calcium phosphate (CaP) or CaCO₃-mineralized nanoparticles based on various templates, including block copolymers, polymer micelles, and mesoporous silica nanoparticles. CaP and CaCO₃ have unique aqueous solution properties: The aqueous solubility of CaP and CaCO₃ is largely dependent on pH level.^[8,9] At physiological pH, they exist as stable crystalline solids, whereas, around or below weak acidic pH, they dissociated as non-toxic ionic species. Based on this aqueous property, CaCO₃ has been used as absorbable templates for fabrication of hybrid colloidal spheres.^[10] Additionally, CaCO₃ minerals react with the proton (H⁺) and decompose to generate carbon dioxide (CO₂) gas in an acid environment.^[9] Using this unique gas-generating property of CaCO₃ minerals, we have recently suggested a novel concept of CaCO₃ mineralized nanoparticles that could serve as a US imaging contrast agents.^[8c]

Photodynamic therapy (PDT) has emerged as an alternative to common therapies such as surgery, chemotherapy, and

^a Department of Life and Nanopharmaceutical Science, College of Pharmacy, Kyung Hee University, Seoul 130-701, Korea.

^b Department of Maxillofacial Biomedical Engineering & Institute of Oral Biology, School of Dentistry, Kyung Hee University, Seoul 130-701, Korea.
E-mail: schlee@khu.ac.kr

^c Center for Theragnosis, Biomedical Research Institute, Korea Institute of Science and Technology, Seoul 136-791, Korea.

[†] These authors contributed equally to this paper.

Electronic Supplementary Information (ESI) available: [details of any supplementary information available should be included here]. See DOI: 10.1039/x0xx00000x

radiotherapy, since it is a non-invasive method and a relatively painless treatment for patients.^[11] Moreover, the photosensitizer in PDT only acts as a cytotoxic agent when irradiated with the proper wavelength of light. Upon light irradiation, the photosensitizers transfer energy to tissue oxygen, leading to production of singlet oxygen and free radical, which cause serious cellular toxicity.^[12] However, there are limitations of photosensitizers for clinical application due to their low selectivity to target tumor tissues, thereby causing prolonged phototoxicity at the normal tissues.^[13] To prevent skin and eye phototoxicity, patients are recommended to avoid sunlight exposure during clinical trials for several weeks or months.^[11a,14,15]

To date, diverse nanoparticle systems have been designed to enhance delivery efficacy of photosensitizers into tumoral environments for photodynamic therapy. However, prior to irradiation, identification of the location and size of tumors is a prerequisite. In addition, the photodynamic treatment procedure needs to be monitored in real time during therapy. US imaging can be one of the promising choices to address these requirements.

Therefore, combination of US imaging and photodynamic therapeutic functions into a rationally designed nanoparticle system is a challenging research subject for imaging-guided photodynamic therapy.

Herein, we have developed a novel theranostic agent based on a photosensitizer-loaded pH-responsive bubble-generating nanoparticle fabricated by CaCO₃ mineralization process on the block copolymer (poly(ethylene glycol)-b-poly(L-aspartic acid) (PEG-PAsp)). It can allow for generating CO₂ gas bubbles and simultaneously triggering release of photosensitizers at tumoral acidic pH for US image-guided photodynamic therapy. The extracellular pH (6.4-7.2) in tumor tissues is lower than the extracellular pH in normal tissues (7.4) because of up-regulated glycolysis and insufficient vascular formation, which produced hypoxia extracellular environment.^[16] This difference of pH in the tumor tissue was chosen as a target for tumoral US imaging and PDT. As a model photosensitizer, chlorin e6 (Ce6) was selected on account of its high absorption at long wavelengths and high efficacy of singlet oxygen generation.^[17]

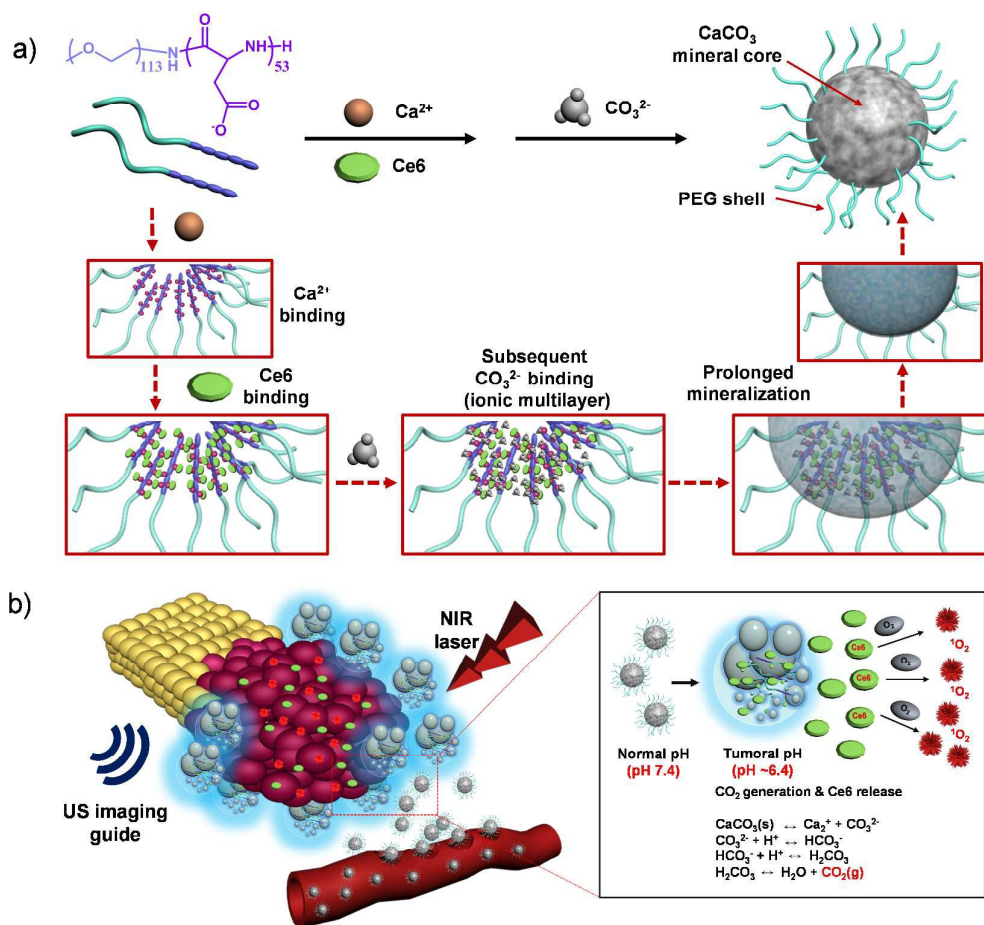


Fig. 1 Schematic illustration of (a) fabrication process of Ce6-BMNs and (b) CO₂ bubble generation for US imaging and subsequent Ce6 release for photodynamic therapy after accumulation of Ce6-BMNs at tumor tissues.

Journal of Materials Chemistry B

ARTICLE

Fig. 1 shows an overall mineralization process for developing of the Ce6-loaded bubble-generating mineralized nanoparticles (Ce6-BMNs) and a postulated working principle of US imaging-guided PDT that shows how the Ce6-BMNs can generate the CO₂ gas bubbles and facilitate Ce6 release at tumoral environments. In this work, we evaluated the potential of the Ce6-BMNs for US imaging-guided PDT. We estimated the pH-controlled gas content from mineralized nanoparticles, *in vitro* US imaging by bubbling generation, and pH-responsive Ce6 release behavior. We also investigated the generation of singlet oxygen of the Ce6-BMNs under pH control. In addition, *in vitro* cell experiments were performed to support cellular uptake, biocompatibility of mineralized nanoparticles, and a phototoxicity of the Ce6-BMNs for MCF-7 breast cancer cells was also evaluated.

Experimental

Materials

α -Methoxy- ω -amino-poly(ethylene glycol) (CH₃O-PEG-NH₂) (M_n = 5000 g/mol) was purchased from IDBIOCHEM Inc. (Seoul, Korea). β -Benzyl L-aspartate (BAsp), *p*-nitroso-*N,N'*-dimethylaniline (RNO), and histidine were purchased from Sigma Co. (St. Louis, MO) and used without further purification. *N,N*-Dimethylformamide (DMF) was dried and distilled over calcium hydride. Chlorin e6 (Ce6) trisodium salt was purchased from Wako Pure chemical Industries, Ltd (Osaka, Japan). Calcium chloride (CaCl₂) and sodium carbonate (Na₂CO₃) were of the reagent grade. β -Benzyl L-aspartate *N*-carboxyanhydride (BAsp-NCA) of high purity was synthesized by the Fuchs-Farthing method using triphosgene.^[18] All other chemicals and solvents were of the analytical grade.

Synthesis of PEG-*b*-PAsp copolymer (PEG-PAsp)

Poly (ethylene glycol)-*b*-poly (L-aspartic acid) (PEG-PAsp) that had EG units of 113 and Asp units of 53 was synthesized by a modified procedure established in our laboratory.^[19] In brief, to a stirred solution of CH₃O-PEG-NH₂ (3 g, 0.6 mmol) in dry DMF (20 mL) was added BAsp-NCA (9 g, 36 mmol) at 35 °C under nitrogen. After 24 h, PEG-PBAsp was isolated by repeated precipitation from DMF into diethyl ether. Yield: 81 %. Finally, hydrolytic deprotection of benzyl groups in PEG-PBAsp was performed by treating the block copolymer (3 g) with 0.1 N NaOH (300 mL). The aqueous solution was then dialyzed using a membrane (Molecular weight cut-off (MWCO): 1,000 g/mol) for 24 h, followed by freeze-drying. ¹H NMR spectroscopy showed that the molar composition ratio of monomeric repeating units in PEG and PAsp was 113:53, and the M_n of PEG-PAsp was calculated to be 11,000 g/mol. Gel permeation chromatography (GPC) analyses showed a narrow molecular weight distribution (M_w/M_n = 1.09).

Preparation of Ce6-loaded bubble-generating mineralized nanoparticles (Ce6-BMNs)

The Ce6-BMNs were prepared by a PEG-PAsp-templated *in situ* mineralization method. In a brief procedure, PEG-PAsp (200 mg, 0.018 mmol) was dissolved in doubly distilled water (4 mL) at pH 8.0 for 1 h, and then mixed with an aqueous CaCl₂ solution (2 mL, 0.95 mmol) under stirring at 800 rpm. After 2 h, Ce6 (20 mg) was subsequently added and stirred in the dark at room temperature for 2 h. To initiate CaCO₃ mineralization, an aqueous solution of Na₂CO₃ (2 mL, 0.95 mmol) was slowly dropped to the mixture, and the solution was stirred at 800 rpm at room temperature for 12 h. The molar concentration ratio of [Asp : Ca²⁺ : CO₃²⁻] was fixed as 1:1:1 for a stoichiometric ratio. To remove unreacted ionic species and unloaded Ce6, the solution was dialyzed for 12 h in distilled water using a membrane (Molecular weight cut-off (MWCO): 3500 g/mol) and then lyophilized to obtain the Ce6-BMNs as a green powder. Ce6-unloaded mineralized nanoparticles were prepared by the identical process except the step of adding Ce6 salts.

Characterization of Ce6-BMNs

For sample preparation, the Ce6-BMNs were dispersed in the phosphate buffered saline (PBS) solution (1 mg/ml, pH 7.4, 37 °C) and sonicated for 10 min using a bath-type sonicator. Dynamic light scattering (DLS) measurements for the hydrodynamic diameter and size distribution of the Ce6-BMNs were performed using a 90 Plus particle size analysis (Brookhaven Instruments Corporation). The scattered light of a vertically polarized He-Ne laser (632.8 nm) was measured at an angle of 90° and was collected on an autocorrelator. The hydrodynamic diameters (*d*) and polydispersity factor of the Ce6-BMNs were calculated by the cumulant method.^[20] The morphology of the Ce6-BMNs was determined by transmission electron microscopy (TEM) (CM30, Philips), operated at an acceleration voltage of 200 kV. Each sample was dissolved in doubly distilled water and dropped on the carbon-coated 200 mesh copper grid. TEM-associated energy-dispersive X-ray photoelectron spectroscopy (TEM-EDX) measurement was carried out using CM30 (Philips) equipped with a DX-4 (EDAX), operated at an acceleration voltage of 200 kV. The selected area of the Ce6-BMNs was evaluated by EDX to reveal atomic components. To evaluate the serum stability, DLS analysis was performed. The Ce6-BMNs (3 mg) was immersed into the mixed solution (50:50, v/v) of the PBS solution (pH 7.4) and fetal bovine serum (FBS). At predetermined time intervals, scattered light intensity (SLI) was analyzed and compared to the initial SLI (SLI₀). For Ce6 loading content, the Ce6-BMNs was dissolved in 1.0 N HCl solutions. The absorbance at 405 nm was measured using a UV-Vis spectrophotometer based on the standard curve of free Ce6 salt. The content of CaCO₃ minerals was determined by assaying the concentration of Ca²⁺ as a complex of Arsenazo III/Ca²⁺ at 656 nm.

pH-Controlled gas generation from Ce6-BMNs

The quantification of generated CO₂ gas from the Ce6-BMNs was performed with a quadruple mass spectrometer (Prisma QME 200, Germany) at room temperature. This instrument was equipped with a Faraday cup detector. The generated gas was analyzed with an emission current of 0.058 mA, electron energy of 8 eV, and resolution of 750. Before measurement, a sample chamber was evacuated with a turbo molecular pump (Pfeiffer vacuum, CA, USA). Aqueous buffer solutions (phosphate buffer of pH 7.4 and pH 6.4, 2 mL) and Ce6-BMNs (20 mg) were placed in the sampler, respectively. The solution in the chamber was frozen under vacuum and thawed after 30 min. As a control, the amount of inherent CO₂ present in the PBS solution (pH 7.4) and the amount of CO₂ from the PEG-PAsp polymer in the PBS solution (pH 7.4, pH 6.4) were also calculated based on an identical procedure.

In vitro Ce6 release from Ce6-BMNs

In vitro release behaviors of Ce6 from the Ce6-BMNs were investigated in the aqueous buffer solution (phosphate buffer of pH 7.4 and pH 6.4). After dispersed in each release media, the Ce6-BMNs (1 mg/ml) were transferred to a dialysis membrane bag (MWCO: 3500 g/mol, Spectra/Por®). The submerged membrane bag in 10 mL of each release medium was shaken at 150 rpm at 37 °C. The release medium (10 mL) was replaced with fresh one at predetermined time intervals. The cumulative amount of Ce6 was analyzed using a UV-Vis spectrometer by calculating the absorbance at 405 nm based on the standard curve obtained using Ce6.

In Vitro US imaging

In vitro US imaging of the Ce6-BMNs was performed in the PBS solutions (pH 7.4 and pH 6.4). A phantom gel plate, made by embedding a 500 µL Eppendorf tube in the agar-gel and then removing the tube after the phantom gel had cooled, was used for *in vitro* US imaging. Echogenic US images were obtained using Visualsonics Vevo 770® (High-Resolution Micro-Imaging System, Visualsonics, Toronto, Canada) with RMV 706 transducer at 40 MHz at a static state. The US images at pH 7.4 and 6.4 was obtained up to 180 min, and, as a normalizing process, the US intensity obtained from the water (control solution) was subtracted from that observed for Ce6-BMNs solutions.

Visualization of CO₂ bubble-generating images from Ce6-BMNs

A drop of the aqueous Ce6-BMNs solution (5 mg/mL, PBS, pH 6.4) was placed on the slide glass. As a control, the sample for an aqueous solution of the Ce6-BMNs (PBS, pH 7.4) was also prepared as described above. The CO₂ bubble-generating images from the Ce6-BMNs were traced for 90 min using optical microscope (IX71; Olympus Co. Ltd., Japan) equipped with 40 × focal lens (Optical magnification is ×400).

Singlet oxygen generation of Ce6-BMNs

The generation of singlet oxygen was detected by oxidation of RNO in the presence of histidine as a singlet oxygen trap.^[21] Aqueous RNO (250 µM, 100 µL) solutions were mixed with the histidine (300 µL, 0.03 M) solution. Free Ce6 (20 µg) or the Ce6-BMNs containing 20 µg of Ce6 were dissolved in each of 700 µL of buffer solutions (phosphate buffer of pH 7.4 and pH6.4). Each solution was added

into the RNO solution containing histidine. The solution was bubbled with water-saturated oxygen for 10 min and then irradiated with a laser (671 nm, 6 Jcm⁻²) for 50 min. The absorbance of RNO was monitored at 440 nm using a spectrophotometer (UV-1650PC). The bleaching of the RNO absorption indicated the generation of singlet oxygen.

Cytotoxicity of PEG-PAsp and BMNs

MCF-7 human breast cancer cells were obtained from the Korean Cell Line Bank (KCLB, Seoul). Cell were cultured in Dulbecco's Modified Eagle's Medium (DMEM, Gibco BRL) containing 10% (v/v) heat-inactivated fetal bovine serum (FBS, Gibco BRL), and 1% (v/v) penicillin-streptomycin (Gibco BRL). Cells were incubated in a humidified incubator at 37°C with 5% CO₂. The medium was replaced every two days. To estimate cell viability, MCF-7 cells were seeded onto 96-well flat-bottomed tissue-culture plate at 5×10³ cells per well in 200 µL of medium, and incubated for 24 h at 37 °C with 5% CO₂. The medium of each well was then replaced by 200 µL of fresh medium containing PEG-PAsp and BMNs at various concentrations from 1 to 1000 µg/mL, and the plates were incubated at 37 °C with 5% CO₂. After 24 h, the medium was removed, and washed with PBS. Cell viability was evaluated by cell counting kit-8 (CCK-8) solutions (Dojindo Laboratories, Kumamoto). The absorbance of each well was measured at 450 nm by a microplate reader (Biorad® Elizer, PA).

Cell phototoxicity

MCF-7 cells were seeded onto 96-well plate at 5×10³ cells per well in 200 µL, and incubated for 24 h at 37 °C with 5% CO₂. The medium of each well was then replaced by 200 µL of fresh medium containing free Ce6 at various concentrations from 0.5 to 10 µg/mL and the Ce6-BMNs (equivalent concentration range of Ce6), and the plates were incubated at 37 °C with 5% CO₂. After 2 h, the medium was removed and washed twice with PBS, and then fresh medium was added. Sample-treated cells were irradiated using LED lamp (670-690 nm, 100 mW/cm²) for 30 min. Cells were incubated for additional 24 h, and then cell viability was determined by CCK-8 solutions.

Intracellular distribution of Ce6-BMNs

To visualize intracellular distribution, MCF-7 cells (2×10⁴ cells per well) were seeded onto 6-well plate in 2 mL of DMEM supplemented with 10% fetal bovine serum (FBS), 1% antibiotics (penicillin 100 U/mM, streptomycin 0.1 mg/mL) and allowed to attach for 24 h. After the medium was removed, cells were treated with LysoTracker (100 nM) and then incubated another 1 h at 37 °C in a CO₂ incubator. The medium was then replaced with 2 mL of fresh medium containing the Ce6-BMNs. The cells were incubated for 0.5 h and 2 h, then rinsed two times with PBS and fixed with 4 wt% paraformaldehyde solution. The confocal laser scanning microscopy (CLSM) images of Ce6-BMNs-treated MCF-7 cells labeled with LysoTracker were obtained by a confocal laser scanning microscope (C1si, Nikon, Japan) by green fluorescing (λ_{ex} = 470-490 nm) and red-fluorescing (λ_{ex} = 520-550 nm).

Live/dead image of Ce6-BMNs-treated cells

MCF-7 cells were seeded onto 24-well cell culture plates at a density of 2×10^4 cells/well in 1 mL of DMEM medium supplemented with 10% FBS, 1% penicillin streptomycin. After 24 h incubation, the culture medium was replaced with 1 mL of medium containing an equivalent Ce6 concentration (5 $\mu\text{g}/\text{mL}$) of free Ce6 and the Ce6-BMNs. After 2 h incubation, the cells were washed three times with the PBS solution, and the fresh medium was added. Cells were then illuminated with a LED lamp (670-690 nm, 100 mW/cm^2) for 30 min and incubated at 37 $^\circ\text{C}$ for 5 h prior to viability staining. Live/dead images were assessed using fluorescence microscopy (IX71, Olympus, Japan) by incubating cells for 5 min in a 200 μL solution of the PBS solution containing 4 mM calcein AM 1 μL for live cells (green) and 2 mM EthD-1 4 μL for dead cell (red).

Results and discussion

Fabrication and characterization of Ce6-BMNs

For fabrication of the Ce6-BMNs, the anionic PEG-PAsp was employed as a template for CaCO_3 mineralization in the presence of calcium cations (Ca^{2+}), carbonate ions (CO_3^{2-}), and a negatively charged Ce6 photosensitizer. The Ce6-BMNs were composed of two distinct domains, the outer PEG shell and the CaCO_3 -mineralized inner core loaded with Ce6. The PEG block formed the hydrated shell and may contribute to the prolonged colloidal stability in the blood stream and decrease the nonspecific interaction with plasma proteins because of the feature of PEG.^[22b,23] Particularly, carboxylate anions in the PAsp domain are the key moieties for nucleation and growth of CaCO_3 core during the mineralization process. As illustrated in Scheme 1a, Ca^{2+} sourced from calcium chloride were preferentially localized in PAsp domains because of electrostatic interaction between Ca^{2+} ions and PAsp carboxylate anions. Subsequent addition of negatively charged Ce6 and CO_3^{2-} anions generated double ionic layers adjacent to PAsp surfaces, leading to a partial supersaturation, which act as a driving force of nucleating and growth of CaCO_3 mineral cores. To obtain uniform mineralized nanoparticles by preventing uncontrolled growth of CaCO_3 crystals, we fixed a stoichiometric molar ratio of [Asp : Ca^{2+} : CO_3^{2-}] at 1 : 1 : 1. Our previous observations verified that the molar ratio of [Asp] to [Ca^{2+}]/[CO_3^{2-}] was a determining factor for fabrication of BMNs with a uniform dimension and morphology.^[8c] During the mineralization process, Ce6 was simply loaded into the inner CaCO_3 core *in situ* through the ionic interactions. The successful loading of Ce6 was confirmed by UV-Vis spectroscopy. The UV-Vis spectrum indicates that the Ce6-BMNs exhibited two main peaks of absorbance at 405 nm and 655 nm, which was originated from free Ce6 (Fig. S1 in the ESI). The content of CaCO_3 in the Ce6-BMNs was estimated to be 32.8 wt%. The loading content and loading efficiency of Ce6 were calculated to be 8.3 wt% and 83.3%, respectively (Table S1). The mean hydrodynamic diameter of the Ce6-BMNs, measured by dynamic light scattering (DLS), was estimated to be 354.0 nm (Table S1). Transmission electron microscopy (TEM) analysis (Fig. 2a) shows that the Ce6-BMNs have spherical and uniform structure. TEM images indicated that the size of the Ce6-BMNs was around 300 nm, which was a consistent range compared with the hydrodynamic diameter determined by DLS. TEM-associated energy-dispersive X-ray spectroscopy (EDX)

confirmed that the Ce6-BMNs mainly contained Ca, C, and O, which are the elements of CaCO_3 minerals (Fig. 2b). TEM-associated selected-area electron diffraction (SAED) analysis shows that the Ce6-BMNs had a vaterite crystalline structure (Fig. 1a). Fourier transform infrared (FT-IR) analysis supported that the Ce6-BMNs showed the existence of CaCO_3 crystalline structure in a vaterite polymorph as showing stretching band at 877 and 746 cm^{-1} (Fig. 2c).^[8c,24]

Ideally, the pH-responsive nanoparticle need to maintain the nano-sized structure and minimize the loss of loaded payloads in the bloodstream, and also can facilitate release them within the target tumoral acidic environment for successful treatment. Serum proteins of the blood components are known as major species that destabilize the nanoparticle structure before it reaches target tissues when the nanoparticles are administered by intravenous injection.^{8a} This circumstance in the bloodstream can cause low delivery efficiency at the target tumor site. Therefore, it is critical to verify the stability of the Ce6-BMNs under serum conditions. To examine the kinetic stability of the Ce6-BMNs in serum solution (50% fetal bovine serum (FBS) in a PBS solution), DLS analysis was used. As shown in Fig. S2 in the ESI, time-dependent change of the ratio of scattered light intensities (SLI/SLI_0) of the Ce6-BMNs did not show any significant changes for 3 days due to the robust structure of vaterite CaCO_3 mineral cores at pH 7.4. This results indicated that the serum protein cannot change or destabilize the structures of the Ce6-BMNs. Thus, the CaCO_3 mineral cores could effectively hold Ce6 in the core domains and maintain the robustness of nanoparticle structure as well as prevent the collapse of the particles *in vivo* blood stream. In addition, the outer PEG shell may also contribute to the prolonged colloidal stability of Ce6-BMNs due to its hydrated structure in aqueous media.

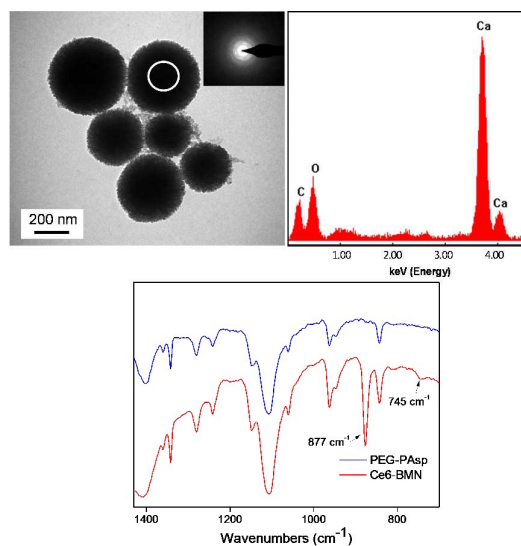


Fig. 2 (a) TEM image and TEM-associated SAED pattern of CaCO_3 cores of Ce6-BMNs and (b) TEM-associated EDX data. The white circle in Fig. 2a indicates the selected area for SAED and EDX analyses. (c) FT-IR data of PEG-PAsp and Ce6-BMNs.

Gas content from Ce6-BMNs

The contents of generated CO₂ gas from the Ce6-BMNs under the pH control at 37 °C was quantified using a mass spectrometer. As shown in Fig. 3, the amount of CO₂ present in the pH 7.4 buffer solution (0.020 cc/atm) was estimated as a control. There was no meaningful difference between the amount of CO₂ from PEG-PAsp (pH 7.4 (0.020 cc/atm) and pH 6.4 (0.019 cc/atm)) and the amount of CO₂ in pH 7.4 buffer solution, indicating the PEG-PAsp polymer itself generated no CO₂ bubble at pH 7.4 and pH 6.4. Interestingly, the Ce6-BMNs at pH 6.4 generated considerable contents of CO₂ gas (0.076 cc/atm), whereas the gas content of the Ce6-BMNs at pH 7.4 was only 0.025 cc/atm, which indicated the negligible amount of generated CO₂ comparable to the control groups. These results were supported by the previous report in the literature for aqueous CaCO₃ chemical equilibria describing that, when the pH level decreased, the CaCO₃ mineral reacted with acids, producing carbonic acid that generates CO₂ gas.^[25]

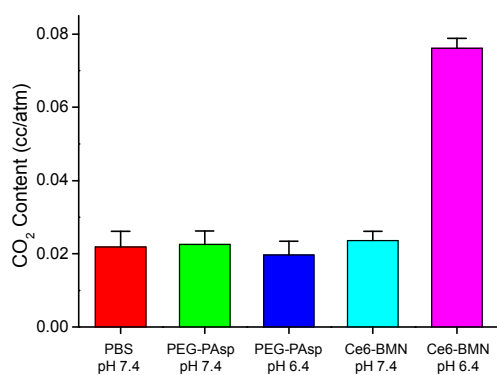


Fig. 3 The amount of CO₂ generated from Ce6-BMNs at various pH.

Visualization of bubble generation

To confirm the pH-responsive bubble generation, the Ce6-BMNs in the buffer solutions (pH 7.4 and 6.4) were time-dependently visualized using optical microscopy (Fig. S3 in the ESI). As a control, the Ce6-BMNs at pH 7.4 did not exhibit particular morphological change, and any bubble formation was not observed for 90 min (data not shown). In contrast, we observed that the Ce6-BMNs at pH 6.4 formed micro-sized bubbles at 30 min. Furthermore, the size of bubble generated from the mineralized Ce6-NPs gradually grew up to about 10 μm at 90 min, which indicated generated CO₂ bubbles from the Ce6-BMNs. Based on this result, we demonstrated that the pH-responsive Ce6-BMNs generated micro-sized bubbles for effective echogenic US imaging.

pH-Responsive *in vitro* echogenic properties of Ce6-BMNs

To ascertain the potential of the Ce6-BMNs as US contrast agents, we estimated *in vitro* US echogenic characteristics of Ce6-BMNs (Fig. 4). The Ce6-BMNs at pH 7.4 did not show any substantial acoustic reflectivity contrast under a US field, because the Ce6-BMNs did not generate sufficient CO₂ gas for microbubble formation. This observation is consistent with the results of the pH-dependent quantification assay of CO₂ generation (Fig. 3). Noticeably, the US contrast images of the Ce6-BMNs were

significantly enhanced at weakly acidic pH condition (pH 6.4). The extended US images could be obtained possibly due to the slow rate of dissolution of CaCO₃ cores at pH 6.4. This long-term acoustic reflectivity is desirable for more accurate imaging of the tumor tissues of interest. This pH-dependent echogenic US image is in accordance with the gas content and the microscopic bubble-generating image of the Ce6-BMNs. The contrast enhancement of the Ce6-BMNs at a specific cellular pH (tumoral acidic pH 6.4) showed that the generation of CO₂ bubbles was responsible for the resonance under a US field. In particular, by utilizing pH-responsive bubble-generating feature of this Ce6-BMNs, we were able to identify tumoral regions from normal tissues at a real time under US imaging, which provide the guidance of Ce6-based photodynamic therapy for tumors simultaneously.

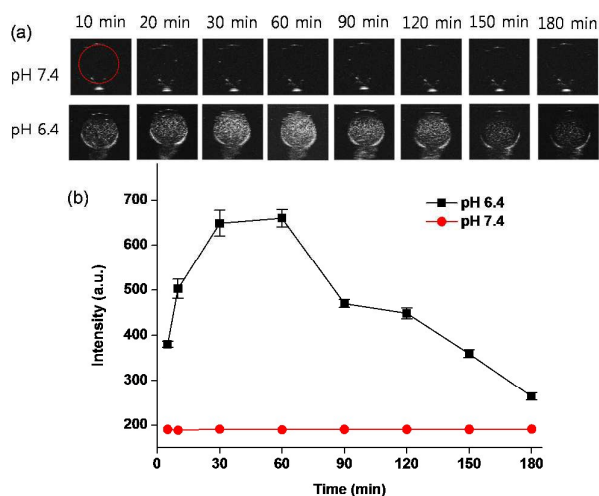


Fig. 4 (a) Time-dependent *in vitro* US images and (b) US contrast intensity from Ce6-BMNs at various pH.

In vitro pH-responsive Ce6 release from Ce6-BMNs

To date, diverse classes of stimuli-responsive nanocarriers have been developed for improving anticancer therapeutic activity.^[26,27] Of various systems, pH-responsive nanocarriers have been designed mostly based on organic polymers with acid-labile linkers, such as acetal, ketal, and citraconic amides.^[19,28,29] CaCO₃, as an inorganic material, may display the pH-responsive controlled drug-releasing property. According to the chemical equilibrium of CaCO₃ in the aqueous phase (Fig. 1b), the CaCO₃ mineral has a pH-dependent aqueous solubility and dissolves with generating CO₂ gas below weak acidic pH, whereas it can maintain the solid mineral state at physiological pH (pH 7.4). Therefore, the mineralized CaCO₃ core is expected to improve the particle structure as well as hold loaded Ce6 at physiological pH, while degrades at the tumoral acidic pH to trigger encapsulated Ce6.

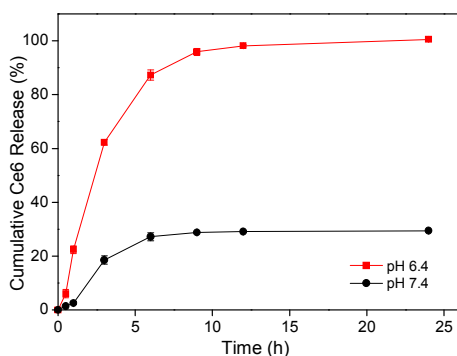


Fig. 5. *In vitro* pH-dependent Ce6 release profiles from Ce6-BMNs.

For a high efficacy of PDT, the photosensitizer-loaded nanocarriers need to be dissociated at tumor environments because the photosensitizers loaded at the core domains of the nanocarriers may undergo the intramolecular energy transfer, which leads to the reduced singlet oxygen generation. We examined the pH-dependent *in vitro* Ce6 release profile of Ce6-BMNs in aqueous buffer solutions (pH 7.4 and 6.4) (Fig. 5). These data showed that, at pH 7.4, the Ce6-BMNs effectively retarded Ce6 release even after 24 h, which is attributed to the low solubility of CaCO_3 . On the other hand, Ce6 was released rapidly from the Ce6-BMNs at tumoral acidic pH (pH 6.4) by 98% within 12 h, indicating that CaCO_3 mineral core reacts with acids to produce carbonic acid, thereby making CaCO_3 more soluble, which could trigger the effective Ce6 release.

In vitro singlet oxygen generation of Ce6-BMNs

Fig. 6 shows the time-dependent monitoring of singlet oxygen generation from the Ce6-BMNs in the presence of RNO and histidine. The RNO assay is a useful in detecting oxidation of RNO in the presence of imidazole as a result of singlet oxygen production.^[30] Generation of singlet oxygen from the Ce6-BMNs leads to reaction with imidazole-containing histidine to form a peroxide intermediate, which subsequently oxidize RNO to cause bleaching of RNO absorbance. After being exposed to light, free Ce6 sharply decreased in the RNO concentration at both pH 6.4 and 7.4 buffer solution, demonstrating rapid generation of singlet oxygen. However, the solution of the Ce6-BMNs at pH 7.4 showed retarded decrease compared to free Ce6, indicating some of the loaded Ce6 may form intermolecular aggregates and underwent self-quenching, which hinder the singlet oxygen generation from the Ce6 of Ce6-BMNs. Notably, at pH 6.4, the rate of singlet oxygen generation from loaded Ce6 in the Ce6-BMNs increased to a similar level to that from free Ce6, suggesting that encapsulated Ce6 was released from Ce6-BMNs by dissolution of CaCO_3 cores to recover its inherent fluorescence of monomeric structures.

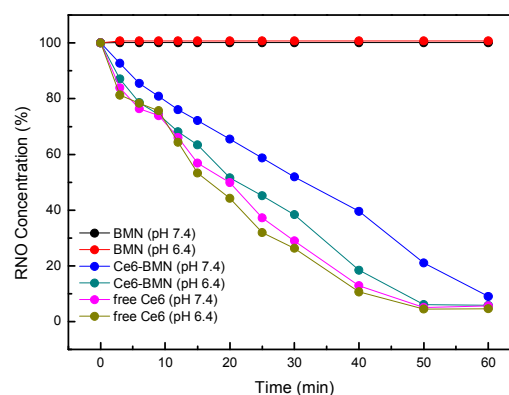


Fig. 6. Singlet oxygen generation determined using RNO as an indicator as a function of irradiation time.

In vitro laser-mediated phototoxicity of Ce6-BMNs

Next, we evaluated cell viability of PEG-PAsp and Ce6-free BMNs at various concentrations using MCF-7 human breast cancer cells (Fig. 7). Both PEG-PAsp and BMNs were not cytotoxic up to 250 $\mu\text{g}/\text{mL}$.

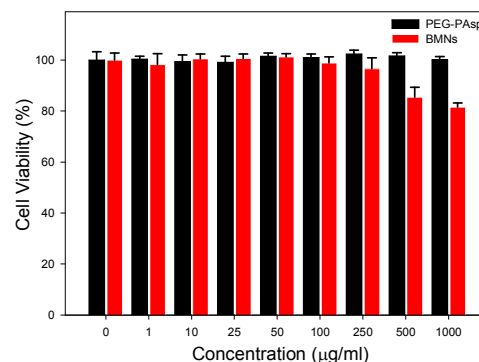


Fig. 7 *In vitro* cytotoxicity of PEG-PAsp and BMNs without irradiation after 24 h incubation. Results represent means \pm SDs (n=3)

Although the cell viability slightly decreased with increasing the concentration of BMNs, this result is acceptable for laser-mediated phototoxicity test because we carried out that experiment under 250 $\mu\text{g}/\text{mL}$ of BMNs.

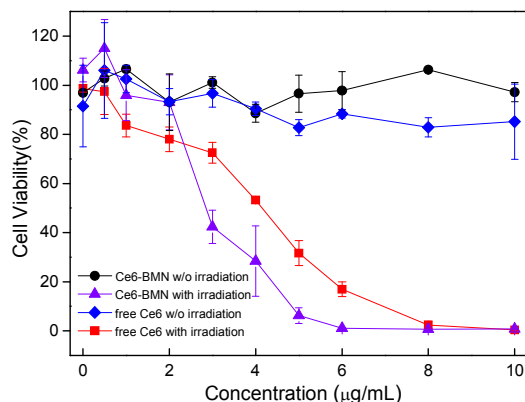


Figure 8. *In vitro* phototoxicity of free Ce6 and Ce6-BMNs with or

without irradiation after 24 h. Results represent means \pm SDs (n=5)

We estimated *in vitro* phototoxicity of the Ce6-BMNs and free Ce6 for MCF-7 cells with and without light irradiation. As shown in Fig. 8, cytotoxicity was not observed in the case of non-irradiated Ce6-BMNs and free Ce6. However, irradiated with an adequate amount of near-infrared (NIR) wavelengths of laser for 30 min, MCF-7 cells showed phototoxicity according to the concentration of Ce6 in each sample. It is of great importance to note that the phototoxicity of the Ce6-BMNs was generally higher than that of free Ce6, which indicated that the Ce6-BMNs would undergo facile cellular uptake in comparison with negatively charge free Ce6. Therefore, we can suggest that the Ce6-BMNs might be useful in PDT, because Ce6-loaded mineralized nanoparticles may maintain a robust structure and minimize Ce6 loss in the blood for a high delivery efficacy, thereby resulting in enhanced therapeutic activity at the target tumor site.

Intracellular distribution of Ce6-BMNs

We observed the intracellular uptake of the Ce6-BMNs using confocal laser scanning microscopy (CLSM). Green-fluorescent LysoTracker was used as a marker of acidic cellular endosome. As shown in Fig. S4 in the ESI, after 30 min of incubation, MCF-7 cells treated with the Ce6-BMNs showed low intensity of red fluorescence within the acidic cytoplasm because of the intermolecular aggregates and self-quenching of loaded Ce6 in the CaCO₃ mineral core. This result suggested the endocytosis of Ce6-BMNs and preferential localization within acidic environments, in which the CaCO₃ mineral core would dissolve to accelerate Ce6 release. Furthermore, after incubation for 2 hours, MCF-7 cells treated with the Ce6-BMNs presented homogeneous distribution of strong red fluorescence in the cytoplasm, indicating that a large amount of Ce6 releasing from the Ce6-BMNs by the acidic environment has been diffused to the cytoplasm. These results demonstrated that CaCO₃ mineralized nanoparticles could efficiently deliver Ce6 into the cytoplasm of cancer cells.

Live/dead image of Ce6-BMNs-treated cells

To visualize the laser-triggered PDT effect of the Ce6-BMNs, fluorescence microscopic images of calcein-AM & EthD-1 double stained (live and dead cells) MCF-7 cells were obtained (Fig. 9).

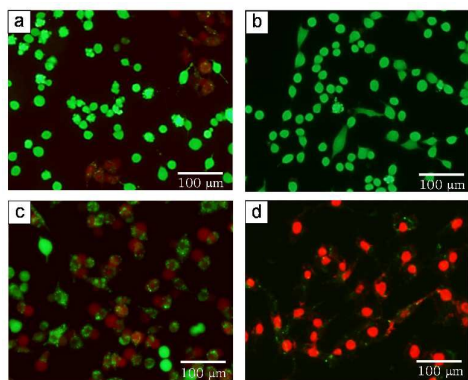


Figure 9. Live/dead cell viability staining of MCF-7 cells incubated with (a) free Ce6 (w/o irradiation), (b) Ce6-BMNs (w/o irradiation),

(c) free Ce6 (with irradiation), and (d) Ce6-BMNs (with irradiation).

For the control groups, where the cells were incubated with free Ce6 or the Ce6-BMNs without light irradiation, negligible cell death (red fluorescence) was observed (Fig. 9a and b). However, upon light irradiation for 30 min, the Ce6-BMNs-treated cells showed remarkably increased cell death by expressing strong red fluorescence compared with free Ce6 treated cells (Fig. 9c and d). Eventually, according to the results of intracellular distribution (Fig. S4 in the ESI) and phototoxicity test (Fig. 8), this different PDT efficacy between free Ce6 and the Ce6-BMNs indicates that the enhanced cellular uptake of Ce6 molecules loaded in the nano-sized Ce6-BMNs is responsible for the improved PDT activity.

Conclusions

We successfully constructed the photosensitizer-loaded mineralized nanoparticles (Ce6-BMNs) composed of bubble-generating CaCO₃ cores for contrast-enhanced diagnostic US imaging and NIR-absorbing photosensitizers for remote photodynamic therapy. The Ce6-BMNs generated CO₂ bubbles at the tumoral pH level, which resonated under a US field with triggering the release of Ce6 to photodynamically destruct MCF- cancer cells. Simultaneous CO₂ bubble generating and Ce6 releasing from the Ce6-BMNs at the tumoral pH could serve as a useful feature for US image-guided PDT for tumors. This simple and highly efficient mineralized nanoparticles would serve as a useful theranostic agent for imaging-guided PDT for various tumors.

Acknowledgement

This work was supported by the National Research Foundation of Korea (NRF) grant funded by the Korea government (MSIP) (No. 2012R1A5A2051388) and was supported by a grant of the Korea Health Technology R&D project (HI14C0175) through the KHIDI funded by the Ministry of Health & Welfare, Republic of Korea.

Notes and references

- 1 a) S. M. Janib, A. S. Moses and J. A. MacKay, *Adv. Drug Deliv. Rev.*, 2010, **62**, 1052-1063; b) C. Tassa, S. Y. Ahaw and R. Weissleder, *Acc. Chem. Res.*, 2011, **44**, 842-852; c) H. Ke, J. Wang, Z. Dai, Y. Jin, E. Qu, Z. Xing, C. Guo, X. Yue and J. Liu, *Angew. Chem. Int. Ed.*, 2011, **50**, 3017-3021.
- 2 a) Y. Xiao, H. Hong, V. Z. Matson, A. Javadi, W. Xu, Y. Yang, Y. Zhang, J. W. Engle, R. J. Nickles and W. Cai, *Theranostics*, 2012, **2**, 757; b) D. Yoo, J.-H. Lee, T.-H. Shin and J. Cheon, *Acc. Chem. Res.*, 2011, **44**, 863-874.
- 3 a) J. R. Lindner, *Nature Rev. Drug Discov.*, 2004, **3**, 527-533.
- 4 a) E. G. Schutt, D. H. Klein, R. M. Mattrey and J. G. Riess, *Angew. Chem. Int. Ed.*, 2003, **42**, 3218-3235; b) K. Ferrara, R. Pollard and M. Borden, *Annu. Rev. Biomed. Eng.*, 2007, **9**, 415-447; c) F. Kiessling, J. Gaetjens and M. Palmowski, *Theranostics*, 2011, **1**, 127-134.
- 5 a) J. A. Straub, D. E. Chickering, C. C. Church, B. Shah, T. Hanlon and H. Bernstein, *J. Controlled Rel.*, 2005, **108**, 21-32; b) M. A. Wheatley, F. Forsberg, K. Oum, R. Ro and D. El-Sherif, *Ultrasonics*, 2006, **44**, 360-367.

- 6 a) S. H. Bloch, M. Wan, P. A. Dayton and K. W. Ferrara, *App. Phys. Lett.*, 2004, **84**, 631-633; b) H. S. Min, E. Kang, H. Koo, J. Lee, K. Kim, R.-W. Park, I.-S. Kim, Y. Choi, I. C. Kwon and M. Han, *Biomaterials*, 2012, **33**, 936-944.
- 7 a) J. K. Willmann, R. H. Kimura, N. Deshpande, A. M. Lutz, J. R. Cochran and S. S. Gambhir, *J. Nuclear Med.*, 2010, **51**, 433-440; b) A. Igaru and S. S. Gambhir, *Am. J. Roentgenol.*, 2013, **201**, W183-W191; c) S. R. Wilson and P. N. Burns, *Radiology*, 2010, **257**, 24-39.
- 8 a) K. H. Min, H. J. Lee, K. Kim, I. C. Kwon, S. Y. Jeong and S. C. Lee, *Biomaterials*, 2012, **33**, 5788-5797; b) H. P. Rim, K. H. Min, H. J. Lee, S. Y. Jeong and S. C. Lee, *Angew. Chem. Int. Ed.*, 2011, **50**, 8853-8857; c) K. H. Min, H. S. Min, H. J. Lee, D. J. Park, J. Y. Yhee, K. Kim, I. C. Kwon, S. Y. Jeong, O. F. Silvestre, X. Chen, Y.-G. Hwang, E.-C. Kim and S. C. Lee, *ACS Nano* 2015, **9**, 134-145; d) H. J. Lee, S. E. Kim, I. K. Keun, C. Park, C. Kim, J. Yang and S. C. Lee, *Chem. Commun.*, 2010, **46**, 377-379.
- 9 a) B. Choi, H. Park, S. Hwang and J. Park, *Int. J. Pharmaceut.*, 2002, **239**, 81-91; b) Q. Yang, S. Wang, P. Fan, L. Wang, Y. Di, K. Lin and F.-S. Xiao, *Chem. Mater.*, 2005, **17**, 5999-6003; c) D. Ogomi, T. Serizawa and M. Akashi, *J. Controlled Rel.*, 2005, **103**, 315-323.
- 10 X. Yan, J. Li and H. Möhwald, *Adv. Mater.*, 2012, **24**, 2663-2667.
- 11 a) S. B. Brown, E. A. Brown and I. Walker, *Lancet Oncol.*, 2004, **5**, 497-508; b) M. Triesscheijn, P. Baas, J. H. Schellens and F. A. Stewart, *Oncologist*, 2006, **11**, 1034-1044; c) H. I. Pass, *J. Nat. Cancer Inst.*, 1993, **85**, 443-456
- 12 L. K. Folkess; and P. Wardman, *Cancer Res.*, 2003, **63**, 776-779.
- 13 Y. Choi, J. R. McCarthy, R. Weissleder and C. H. Tung, *ChemMedChem* 2006, **1**, 458-463.
- 14 R. Ackroyd, C. Kelty, N. Brown and M. Reed, *Photochem. Photobiol.*, 2001, **74**, 656-669.
- 15 K. Chen, A. Preuss, S. Hackbarth, M. Wacker, K. Langer and B. Röder, *J. Photochem. Photobiol. B: Biol.*, 2009, **96**, 66-74.
- 16 a) L. E. Gerweck, S. Vijayappa and S. Kozin, *Mol. Cancer Therapeut.*, 2006, **5**, 1275-1279; b) R. A. Gatenby and R. J. Gillies, *Nature Rev. Cancer* 2004, **4**, 891-899; c) L. E. Gerweck and K. Seetharaman, *Cancer Res.*, 1996, **56**, 1194-1198.
- 17 a) Y. Choi, R. Weissleder and C. H. Tung, *ChemMedChem* 2006, **1**, 698-701; b) W. W. L. Chin, P. W. S. Heng, P. S. P. Thong, R. Bhuvaneshwari, W. Hirt, S. Kuenzel, K. C. Soo and M. Olivo, *European J. Pharmaceut. Biopharmaceut.*, 2008, **69**, 1083-1093.
- 18 W. H. Daly and D. Poché, *Tetrahedron Lett.*, 1988, **29**, 5859-5862.
- 19 S. J. Lee, K. H. Min, H. J. Lee, A. N. Koo, H. P. Rim, B. J. Jeon, S. Y. Jeong, J. S. Heo and S. C. Lee, *Biomacromolecules*, 2011, **12**, 1224-1233.
- 20 A. Harada and K. Kataoka, *Macromolecules*, 1998, **31**, 288-294.
- 21 a) R. Bachor, C. R. Shea, R. Gillies and T. Hasan, *PNAS*, 1991, **88**, 1580-1584; b) H. Y. Yoon, H. Koo, K. Y. Choi, S. J. Lee, K. Kim, I. C. Kwon, J. F. Leary, K. Park, S. H. Yuk and J. H. Park, *Biomaterials*, 2012, **33**, 3980-3989.
- 22 a) T. Gyenes, V. Torma, B. Gyarmati and M. Zrínyi, *Acta Biomater.*, 2008, **4**, 733-744; b) L. Yu, G. T. Chang, H. Zhang and J. D. Ding, *Int. J. Pharmaceut.*, 2008, **348**, 95-106.
- 23 a) K. Y. Choi, H. Y. Yoon, J.-H. Kim, S. M. Bae, R.-W. Park, Y. M. Kang, I.-S. Kim, I. C. Kwon, K. Choi and S. Y. Jeong, *ACS Nano*, 2011, **5**, 8591-8599; b) Y. Tanaka, N. Nishida, M. Sugiyama, M. Kurosaki, K. Matsuura, N. Sakamoto, M. Nakagawa, M. Korenaga K. Hino and S. Hige, *Nature Genetics*, 2009, **41**, 1105-1109.
- 24 K. Naka, Y. Tanaka and Y. Chujo, *Langmuir*, 2002, **18**, 3655-3658.
- 25 S. L. Goss, K. A. Lemons, J. E. Kerstetter and R. H., *J. Pharm. Pharmacol.*, 2007, **59**, 1485-1492.
- 26 F. Zhao, G. Shen, C. Chen, R. Xing, Q. Zou, G. Ma and X. Yan, *Chem. Eur. J.*, 2014, **20**, 6880-6887.
- 27 H. Zhang, J. Fei, X. Yan, A. Wang and J. Li, *Adv. Funct. Mater.*, 2015, **25**, 1193-1204.
- 28 Y. Wu, W. Chen, F. Meng, Z. Wang, R. Cheng, C. Deng, H. Liu and Z. Zhong, *J. Controlled Release*, 2012, **164**, 338-345.
- 29 B. R. Lee, H. J. Baik, N. M. Oh and E. S. Lee, *Polymers*, 2010, **2**, 86-101.
- 30 I. Kraljić and S. E. Mohsni, *Photochemistry and Photobiology*, 1978, **28**, 577-581.

<Graphical Abstract>

Photosensitizer-loaded CaCO_3 -mineralized nanoparticles expressed theranostic potentials for cancer treatment by generating CO_2 bubbles and releasing photosensitizers at tumoral acidic pH for ultrasound imaging and simultaneous photodynamic therapy.

